inorganics

MDPI

Article

Fluorene-Containing β-Diketonato Ligands and Their Rhodium(I) Complexes—A Characterization and Crystallographic Study

Frederick Jacobus Francois Jacobs, Siyanda Khoza and Eleanor Fourie *

Department of Chemistry, Natural and Agricultural Sciences Faculty, University of the Free State, P.O. Box 339, Bloemfontein 9300, South Africa

* Correspondence: fouriee@ufs.ac.za; Tel.: +27-51-401-2071

Abstract

The highly fluorescent fluorene group is of interest for its unique optical and electronic properties. By incorporating it into a metal complex, these properties are extended to the complex and are useful in a number of different applications. Four β-diketone ligands were synthesized containing the fluorene-functional group, where the varying substituent on the β-diketone was CF_3 (**1**), $PhCF_3$ (**2**), Ph (**3**) and $PhCH_3$ (**4**). The corresponding cyclooctadiene rhodium(I) complexes of the type [Rh(cod)((fluorene)COCHCOR)], with R = CF_3 (**5**), $PhCF_3$ (**6**), Ph (**7**) and $PhCH_3$ (**8**) were also synthesized. A crystal structure determination of **2** and **6** was performed, highlighting important changes in the ligand structure as a result of metal complexation. The structure of **2** also showed a hydrogen interaction between the hydroxy and carboxyl groups, forming a pseudo six-membered ring that stabilizes the enol form of the compound. Cyclic voltammetry (CV) of the β-diketones **1**–**4** showed a reduction wave for the reduction of the β-diketonato backbone between −1500 mV and −2100 mV as measured against ferrocene (FcH). CVs of rhodium(I) complexes **5**–**8** showed a reduction of the β-diketonato backbone between −1800 and −2000 mV, as well as an oxidation wave for the oxidation of the rhodium(I) metal centre at approximately 300 mV.

Keywords: fluorene; β-diketone; rhodium (I); crystal structure; cyclic voltammentry

check for updates

Academic Editor: Wolfgang Linert

Received: 30 June 2025
Revised: 23 July 2025
Accepted: 29 July 2025
Published: 30 July 2025

Citation: Jacobs, F.J.F.; Khoza, S.; Fourie, E. Fluorene-Containing β-Diketonato Ligands and Their Rhodium(I) Complexes—A Characterization and Crystallographic Study. *Inorganics* **2025**, *13*, 255. https://doi.org/10.3390/inorganics13080255

Copyright: © 2025 by the authors. Licensee MDPI, Basel, Switzerland. This article is an open access article distributed under the terms and conditions of the Creative Commons Attribution (CC BY) license (https://creativecommons.org/licenses/by/4.0/).

1. Introduction

The fluorene group is considered a very interesting and useful functional group for a number of reasons. It is a highly fluorescent group, as indicated by its name [1]. It is used for this purpose in various ways, as part of light-emitting diodes [2], sensors [3] and electrochromic polymers [4,5]. The fluorene group also displays interesting electronic properties due to its partial aromatic structure. It offers the potential to vary the electronic properties of whatever compound it is part of [6]. It has also been included in complex molecular structures used as hole transporters in solar cells [7].

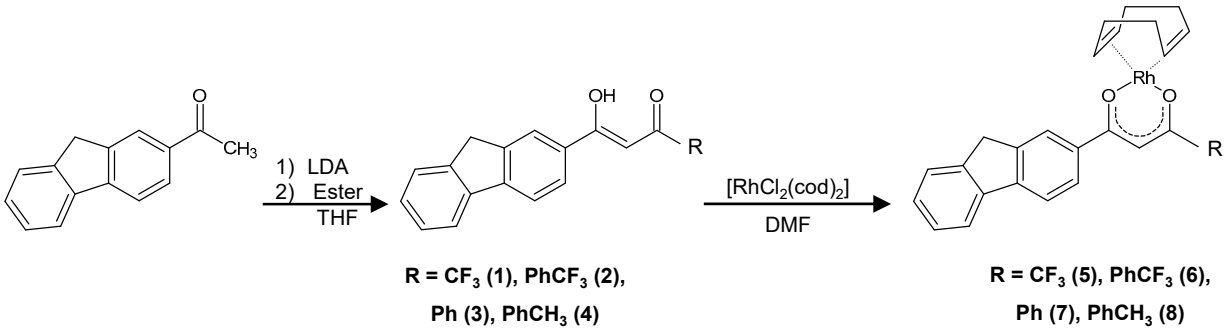
Fluorenes are known to be biologically active or compatibe, and have a number of biological applications. They are commonly employed as a fluorophore in bioimaging [1]. It has been shown that fluorene-9-bisphenol can have neurological effects in mice that influence anxiety [8]. Derivatives of fluorene are also often employed in possible anticancer compounds [9]. Fluorene-containing organic compounds have shown cytotoxic properties on their own [10,11], but also when the fluorene group is incorporated in a ligand system coordinated to a metal [12].

For the purpose of incorporating the fluorene group into more complex molecular structures, it is often modified as a ligand for metal complexation. As a ligand, it has formed part of Schiff base structures, including varied N,O and N,N type Schiff bases [13,14]. These demonstrate notable biological activity as well. The use of Schiff base-type ligands also includes interesting tripodal structures, which aimed to increase the fluorescent properties of the compound [15]. The fluorene group has also been included in N-heterocyclic silver carbene complexes, which form polymeric chains. These complexes were synthesized for the detection of copper(II) in biological environments [16]. Fluorene ligands coordinating through an ethynyl group at the 2,7 and 3,6-positions were synthesized, and complexes with platinum(II) have been investigated for their photophysical and optical power properties [17].

Of interest to us is including the fluorene group into β-diketonato-type ligands, due to its relatively easy synthesis and ability to complex a variety of metals [18,19]. β-Diketone ligands have been reported to possess high fluorescent abilities when complexed to lanthanides [20]. Since the electron-donating ability of the fluorene group is known, we have aimed to investigate the electronic influence further by varying the electron density of the ligand through additional phenyl-based substituents. Similar compounds have been reported as part of boronated compounds with high fluorescent properties [21]. We also complex our newly synthesized β-diketonato ligand with rhodium(I) in order to investigate coordination and electronic properties. In this study, we aim to understand the crystallographic and electrochemical changes when complexing the fluorene-containing ligands to metal complexes. For this reason, the crystallographic study is focused on the structure of a representative ligand **2** and its corresponding metal complex **6**.

2. Results and Discussion

We report the synthesis of four β-diketonato ligands containing the fluorene functional group and their corresponding rhodium(I) cyclooctadiene (cod) complexes. The additional group attached to the β-diketonato backbone was varied through size and electron density, to include CF_3 (**1**), $PhCF_3$ (**2**), Ph (**3**) and $PhCH_3$ (**4**), as shown in Scheme 1.



Scheme 1. The synthetic route used in this study showing the structure of ligands (**1**–**4**) and rhodium(I) complexes (**5**–**8**).

2.1. Synthesis and Characterization

The ligands, **1**–**4** (shown in Scheme 1), were synthesized from acetylfluorene via a Claisen condensation mediated with lithium diisoropylamide (LDA). The ligands were characterized by ^1H and ^{13}C NMR, as well as spectroscopic methods. Compound **3** has been previously reported as part of a highly fluorescent boronated compound [21]. A crystal structure determination was performed on compound **2**, as well as its corresponding rhodium complex, **6**. β-diketones **1**–**4** were isolated through repeated column chromatography (reducing yields to ~20%), as stable off-white crystalline solids. The β-diketones

can exist in either the keto or enol form, which usually exist in equilibrium [22]. The β-diketones **1**–**4** in this study were, however, observed only in the enol form, as evidenced by the α-methine resonance between 6.6 and 6.9 ppm during ^{1}H NMR in $CDCl_3$. FTIR also confirmed the dominance of the enol form, since only a single carbonyl vibrational band was observed between 1580 and 1600 cm^{-1}.

β-Diketonato ligands (**1**–**4**) were complexed with rhodium(I) through reaction with the $[Rh_2Cl_2(cod)_2]$ dimer, as shown in Scheme 1, yielding [Rh(β-diketonato)(cod)] complexes **5**–**8**. This route is preferential for rhodium(I) complexation to electron-rich ligands [23]. The product was precipitated as a crystalline light-yellow powder in a pure form. ^{1}H NMR confirmed the complexation of ligands **1**–**4** with rhodium(I), through a clear up-field shift in methine peaks to 6.4–6.7 ppm. Twelve additional alkyl peaks were also identified between 1.9 and 4.3 ppm, belonging to the cyclooctadiene ligand. Similar observations were made by ^{13}C NMR, where up-field shifts of carbonyl peaks were observed, together with additional peaks belonging to the cod ligand.

2.2. X-Ray Structure Determination

The crystal structures of the β-diketonato ligand **2** {(2Z)-3-(9H-fluoren-2-yl)-3-hydroxy-1-[4-(trifluoromethyl)phenyl]prop-2-en-1-one} and its corresponding rhodium(I) complex **6** {[cycloocta-1,5-diene]-{(2Z)-3-(9H-fluoren-2-yl)-3-hydroxy-1-[4-(trifluoromethyl)phenyl]prop-2-en-1-olato}-rhodium(I)} is reported. The crystal structure of one ligand and one metal complex is reported, as representative of the series, to compare differences between the free ligand and the complexed structure. Since crystallization of the metal complex is challenging, only compound **6** yielded crystals suitable for X-ray diffraction. Subsequently, crystals of the corresponding ligand (compound **2**) were grown and analysed. Illustrated in Figure 1 are line drawings of **2** and **6,** and in Figure 2 are the molecular diagrams of the same.

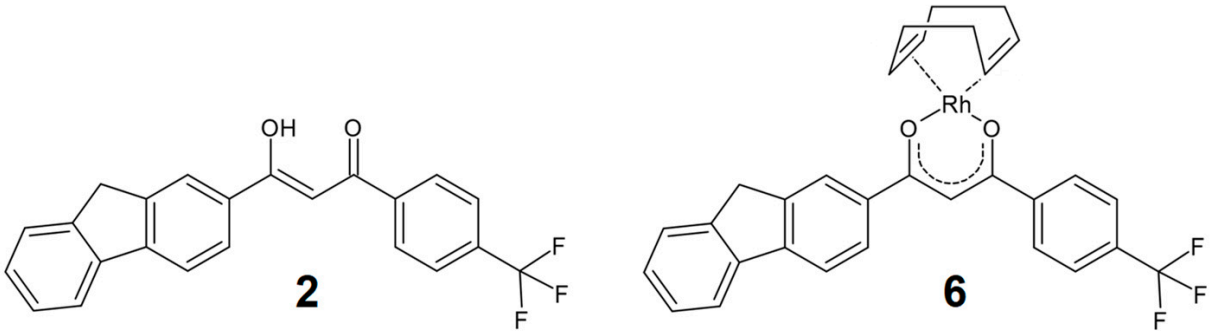


Figure 1. Line drawings of ligand **2** and metal complex **6**.

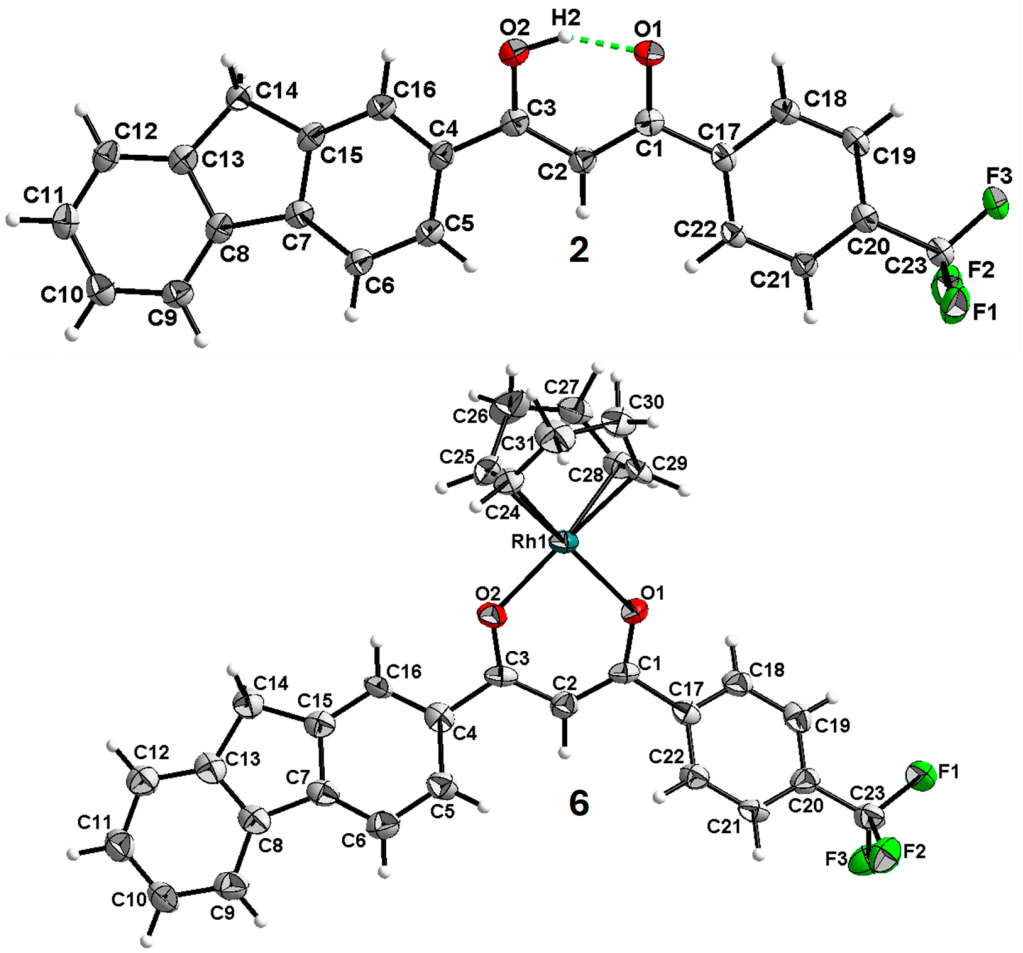


Figure 2. Molecular diagrams of the crystal structures of **2** and **6**. The diagrams contain the atom labels; hydrogen atom labels have been omitted for clarity. All atoms have been drawn at a 50% probability level. Green dashed lines indicate intramolecular hydrogen bonding for **2**. The figures were drawn in DIAMOND [24] (including all subsequent figures, unless stated otherwise).

The crystallographic and refinement parameters for **2** and **6** are listed in Table 1. The ligand **2** crystallized in the orthorhombic *P*bca space group with eight molecules in the unit cell, whereas complex **6** crystallized in the monoclinic crystal system and P21/c space group with four molecules in the unit cell. The ligand contains an intramolecular hydrogen interaction between the hydroxy and carboxyl groups, forming a pseudo-six-membered ring. The stability of this six-membered ring explains the preference for the molecule to exist almost exclusively in the enol form. In the crystal structure of complex **6** it loses this hydrogen interaction and forms a six-membered metallocycle. The metal coordination sphere is completed through the binding of 1,5-cyclooctadiene. Both compounds contain a CF_3 group on the periphery of the ligand system. This functional moiety increases possible application in the biomedical field, since nearly a quarter of all small-molecule drugs that are currently on the market contain fluorine in their structures [25]. The inclusion of the 9H-fluorene group can also enhance the potential for DNA intercalation in possible medical applications [9].

Table 1. General X-ray crystallographic and refinement parameters for **2** and **6**.

Compound	Ligand (2)	Complex (6)
Crystal data		
Chemical formula	$C_{23}H_{15}F_3O_2$	$C_{31}H_{26}F_3O_2Rh$
M_r	380.35	590.43
Crystal system, space group	Orthorhombic, *P*bca	Monoclinic, $P2_1/c$
Temperature (K)	101	100
a, b, c **(Å)**	14.7394(9), 6.0976(4), 37.668(3)	23.920(3), 10.749(2), 9.539(1)
α, β, γ **(°)**	90, 90, 90	90, 91.001(8), 90
V **(Å^3)**	3385.4(4)	2452.6(6)
Z	8	4
μ **(mm^{-1})**	0.988	6.068
Crystal size (mm)	0.239 × 0.048 × 0.001	0.190 × 0.032 × 0.011
Data collection		
Diffractometer	Bruker D8 Venture 4K Kappa Photon III C28 diffractometer	Bruker D8 Venture 4K Kappa Photon III C28 diffractometer
Wavelength (Å)	1.54178 (CuKα)	1.54178 (CuKα)
Absorption correction	Multi-scan *SADABS2016*/2 [3]	Multi-scan *SADABS2016*/2 [3]
T_{min}, T_{max}	0.666, 0.754	0.569, 0.754
No. of measured, independent, and observed [$I > 2\sigma(I)$] reflections	54,753, 3662, 2887	27,666, 5125, 3489
R_{int}	0.0663	0.886
2Θ range for data collection/°	4.692 to 158.948	3.694 to 163.776
Completeness (%)	99.50	99.10
Refinement		
$R [F^2 > 2\sigma(F^2)], wR(F^2), S$	0.0505, 0.1323, 1.043	0.0806, 0.2016, 1.093
No. of reflections	3662	5125
No. of parameters	258	334
$\Delta\rho_{max}, \Delta\rho_{min}$ **(e Å^{-3})**	0.30, −0.32	2.48, −2.01
CCDC No.	2,466,425	2,466,393

Specific bonding distances and angles were selected and compared with similar structures on the Cambridge Structural Database (CSD) [26].

The O1–O2 distances of the ligands were comparably similar, with the value of **2** being 2.434(2) Å and the CSD ligands' values ranging from 2.436(1) Å to 2.529(4) Å (for HUPPOZ, FAXWAD01, ACUVUS, and BICQEM). The same is true for the O1–C1 and O2–C3 with some minor exceptions. The O1–C1 distances for ligand **2** is 1.287(2) Å and the distance range for the other ligands are 1.264(3) Å to 1.295(2) Å for HUPPOZ, FAXWAD01, and ACUVUS, where BICQEM varies significantly with a value of 1.32(1) Å, which can be attributed to the symmetry of this particular molecule, with half being generated by a symmetry element (see [27]). The O2–C3 distance of **2** is 1.301(2) Å and is comparable to the CSD ligands, which have values ranging from 1.295(2) Å to 1.32(1) Å for HUPPOZ, FAXWAD01, ACUVUS, and BICQEM. The C20–C23 distance is 1.499(3) Å for **2** and is identical within standard uncertainty to that of HUPPOZ, which has a value of 1.494(5) Å. The value of FAXWAD01 is slightly longer, since the C23 is saturated with hydrogen atoms as opposed to fluorine atoms, with a value of 1.505(2) Å. The C1–C2–C3 angle is close to 120° for all the ligands, being 119.8(2)°, 122.4(3)°, 119.8(2)°, 120.39(8)°, and 121.12° for **2**, HUPPOZ, FAXWAD01, ACUVUS, and BICQEM, respectively.

The complex's angles and distances are, like those of the ligands, fairly equivalent to one another. The O1–O2 bite distance for **6** is 2.945(7) Å and the CSD metal complex values are 2.849(6) Å, 2.86(1) Å, and 2.910(3) Å for PPDOCR20, CUNZEQ, and WICFUN, respectively. The O1–C1 and O2–C3 distance values are identical within standard uncertainty. The complex **6** has the largest C1–C2–C3 angle of 127.7(8)° where the CSD metal complexes

had values of 125.6(3)°, 124.9(9)°, and 127.1(3)° for PPDOCR20, CUNZEQ, and WICFUN, respectively.

Comparing ligand **2** to metal complex **6** reveals some interesting geometric changes. The O1–O2 distance is significantly longer (2.434(2) Å for **2** and 2.945(7) Å for **6**) while the O1–C1, O2–C3, and C20–C23 distances remain the same within standard uncertainty. As with the larger bite distance, the C1–C2–C3 angle is larger for the metal complex with a value of 127.7(8)° compared to the 119.8(2)° for the ligand.

The distances and angles are tabulated in Table 2.

Table 2. Selected bond distances (Å) and angles (°) for **2**, **6**, and related compounds found in the literature. For ease of comparison, the ligands are shown without shading, while the metal complexes are shaded grey. Line drawings of the crystal structures (which were used for comparison as found on the CSD) are presented in the Supplementary Information associated with this publication.

Compound	Distances (Å)				Angles (°)	Torsion Angles (°)	Reference
	O1–O2	O1–C1	O2–C3	C20–C23	C1–C2–C3	O1–C1–C17–C22	
2	2.434(2)	1.287(2)	1.301(2)	1.499(3)	119.8(2)	159.2(2)	This work
6	2.945(7)	1.28(1)	1.27(1)	1.49(1)	127.7(8)	149.7(9)	This work
HUPPOZ	2.529(4)	1.264(3)	1.310(3)	1.494(5)	122.4(3)	−170.5(3)	[28]
FAXWAD01	2.436(1)	1.295(2)	1.295(2)	1.505(2)	119.8(2)	−172.0(2)	[29]
ACUVUS	2.463(1)	1.278(1)	1.310(1)	N/A	120.39(8)	172.12(8)	[30]
BICQEM	2.52(6)	1.32(1)	1.32(1)	N/A	121.2(4)	−154(1)	[27]
PPDOCR20	2.849(6)	1.283(6)	1.283(6)	N/A	125.6(3)	153.9(5)	[31]
CUNZEQ	2.86(1)	1.30(1)	1.28(1)	N/A	124.9(9)	161.2(9)	[32]
WICFUN	2.910(3)	1.282(3)	1.282(3)	N/A	127.1(3)	153.5(2)	[33]

Ligand **2** and complex **6** both display weak interactions. The weak interactions, i.e., the hydrogen bonding interactions, metal–hydrogen interactions, and π–CH interactions, are listed in Table 3.

Table 3. List of the hydrogen bond, π–CH, and metal–hydrogen interaction parameters of compounds **2** and **6**.

D—H···A	Type of Interaction	D—H (Å)	H···A (Å)	D···A (Å)	D—H···A (°)
(1) Ligand					
O2—H2···O1	H-bond	0.97(2)	1.52(2)	2.434(2)	151(3)
C14—H14A···C9 [i]	π–CH	0.99	2.68	3.639(3)	162(1)
C14—H14B···Cg1 [ii]	π–CH	0.99	3.21	3.875(2)	125.7(1)
(2) Complex					
C21—H21···O1 [iii]	H-bond	0.95	2.50	3.24(1)	134
C22—H22···Rh1 [iv]	Metal-H	0.95	3.07	3.897(9)	146

Symmetry code (s): [(i)] −x + 1, y − 1/2, −z + 3/2; [(ii)] *x*, −*y* + 1/2, *z* + 1/2; [(iii and iv)] *x*, −*y* + 1/2, *z* + 1/2. Cg1 = C17–C22.

The ligand **2** has an intramolecular hydrogen interaction of O2–H2···O1 with a donor to acceptor distance of 2.434(2) Å and a bond angle of 151(3)° (see Figure 3). Comparing this hydrogen bond, which stabilizes the enol form of the ligand with other β-diketones (found in the CSD) shows that they are very similar. HUPPOZ, FAXWAD01, ACUVUS, and BIQEM have donor-to-acceptor distances of 2.529(4) Å, 2.436(1) Å, 2.463(1) Å, and 2.52(6) Å, respectively, and their hydrogen bond angles are 149(2)°, 162(5)°, 157(2)°, and 147(8)°, respectively. Ligand **2** has two π-type interactions with the CH_2 group and adjacent aromatic groups. The C14–H14A··· C9 interaction uses the −x + 1, y − 1/2, −z + 3/2 symmetry operator with a donor-to-aromatic distance of 3.639(3)Å and an angle of 162(1)°. The C14–H14B···Cg1 interaction uses the x, −y + 1/2, z + 1/2 symmetry operator, having a

donor-to-aromatic distance of 3.875(2) Å and an angle of 125.7(1)°. The π–CH interactions are illustrated in Figure 3.

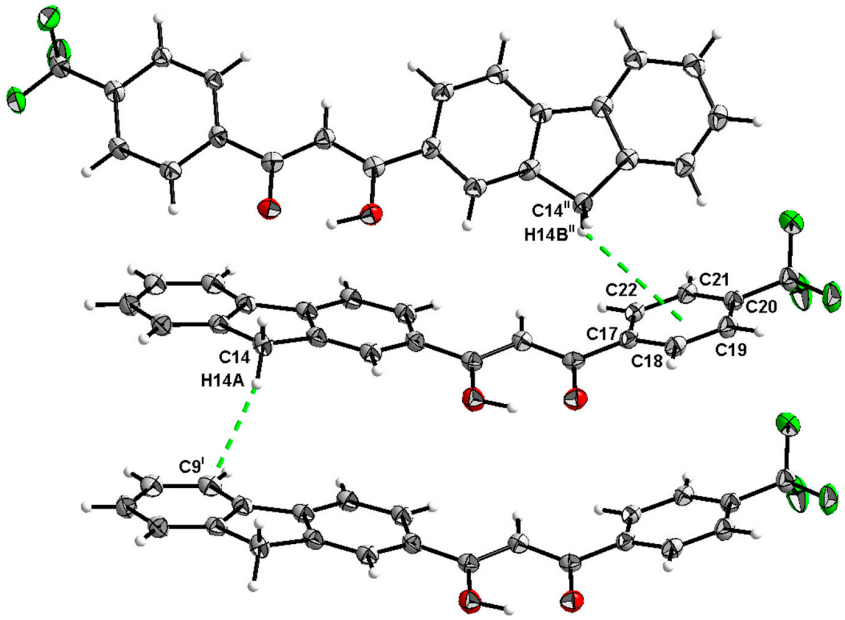


Figure 3. Graphical depiction of the π–CH interactions observed in compound **2**. The interactions are shown in green dashed lines between the donating hydrogen atom and the participating aromatic centroid or carbon atom.

The metal complex **6** has two hydrogen-type interactions. The first is C21–H21···O1 (with a donor to acceptor distance of 3.24(1) Å and an angle of 134°) and the second is C22–H22···Rh1 (with a donor to acceptor distance of 3.897(9) Å and an angle of 146°). Both interactions use the same symmetry operator, which is x, −y + 1/2, z + 1/2. These interactions can be seen in Figure 4.

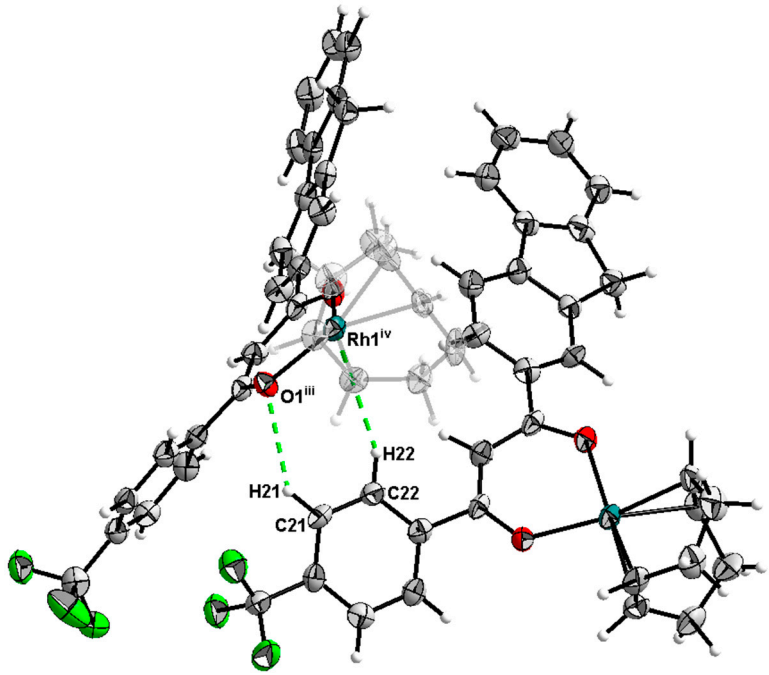


Figure 4. Indicated is the hydrogen interaction and metal–hydrogen interaction as seen in compound **6**. The interactions are drawn as green dashed lines. The obstructing cyclooctadiene ligand is drawn opaquely for clarity.

Upon metal binding, the ligand experiences significant out-of-plane bending of its aromatic regions. This can be quantified by measuring the angle produced between each of the aromatic regions of the molecule. In turn, this can be compared between the two molecules. There are three aromatic regions that can be described and are colored and numbered identically for both structures. The red plane is defined by the C4, C5, C6, C7, C15, and C16 atoms, the green plane by O1, C1, C2, C3, and O2, and the blue plane by C17, C18, C19, C20, C21 and C22. Graphical representation of these planes for ligand **2** can be seen in Figure 5, and the planes of complex **6** are shown in Figure 6.

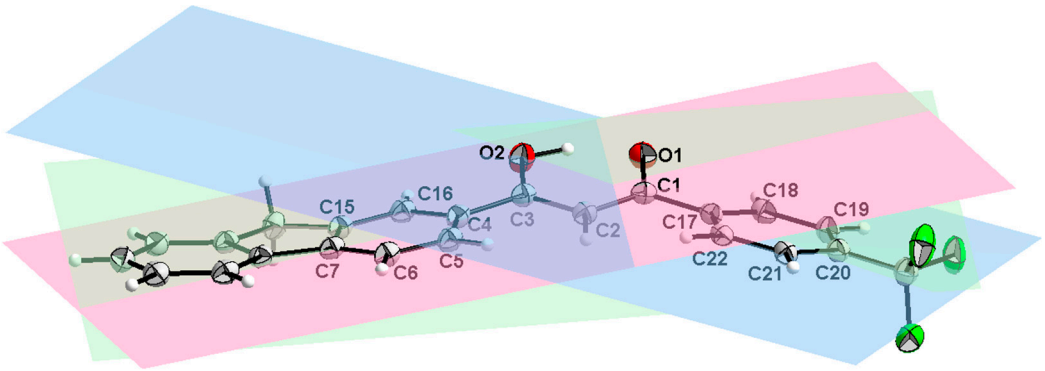


Figure 5. This image depicts the three major planes in compound **2**. The red plane was generated by atoms C4, C5, C6, C7, C15, and C16, the blue plane was generated by atoms C17–C22 and the green plane by O1, C1, C2, C3, and O2.

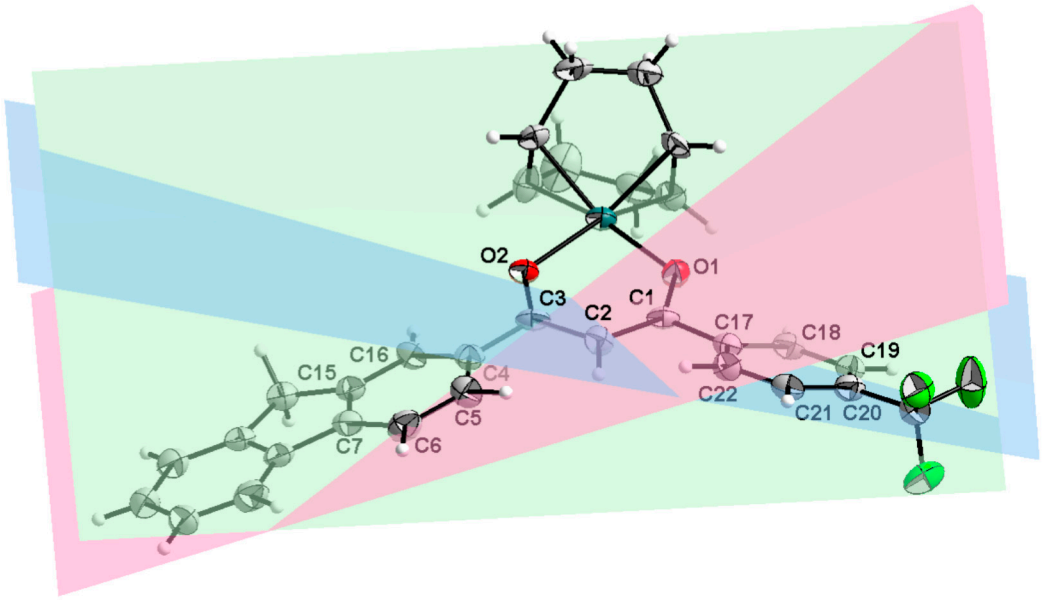


Figure 6. The three major planes in compound **6** are illustrated. The red plane was generated by atoms C4, C5, C6, C7, C15, and C16. The blue plane was generated by atoms C17–C22 and the green plane by O1, C1, C2, C3, and O2.

The red–green plane angle is 18.6(1)° for ligand **2** and is considerably less than the 24.7(3)° for complex **6**. This is true for the green–blue plane angles, 21.5(1)° for **2** and 30.7(3)° for **6**. The largest angle difference is seen in the red–blue angles, which are 17.7(3)° for (1) and 30.8(3)° for **6**. The differences can be ascribed to the coordination of the metal, which induces geometric stress on the ligand, which in turn results in out-of-plane bending. This kind of structural bending could be useful in structure-based drug design, allowing medicinal chemists to fine tune the fit of the potential drug into the active site of the target biological molecule. The planes with their associated angles are listed in Table 4.

Table 4. Listing of the values produced when measuring the angle between the planes of ligand **2** and complex **6**.

Planes	Atoms Used to Generate the Plane	Ligand 2 (°)	Complex 6 (°)
Red—Green	**C4, C5, C6, C7, C15, and C16**	18.6(1)	24.7(3)
Green—Blue	**O1, C1, C2, C3, and O2**	21.5(1)	30.7(3)
Red—Blue	**C17, C18, C19, C20, C21 and C22**	17.7(3)	30.8(3)

The effect on the geometry of the structure can also be seen graphically when ligand **2** and complex **6** are overlayed. The ligands aromatic regions are bent along the plane of the paper away from the metal. This is shown in Figure 7 where the complex is drawn in red and the ligand in green.

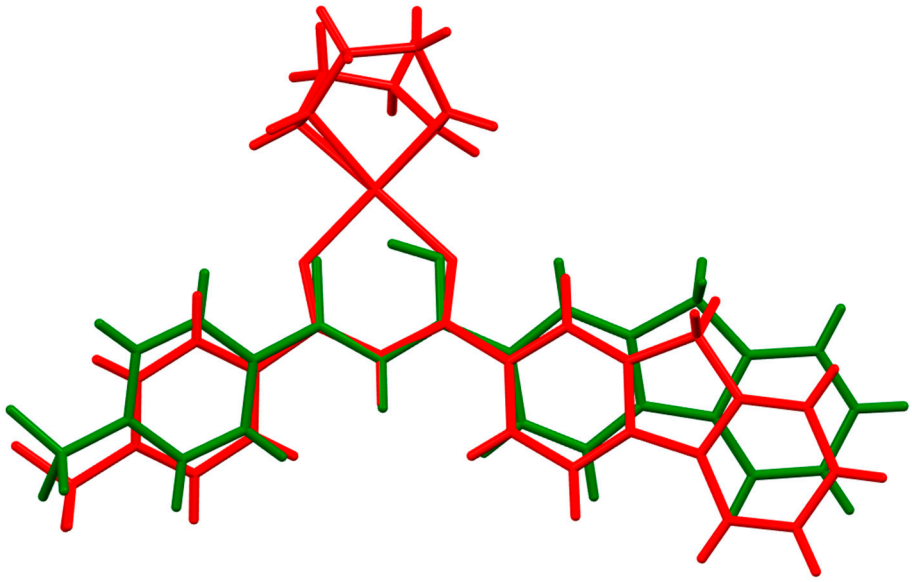
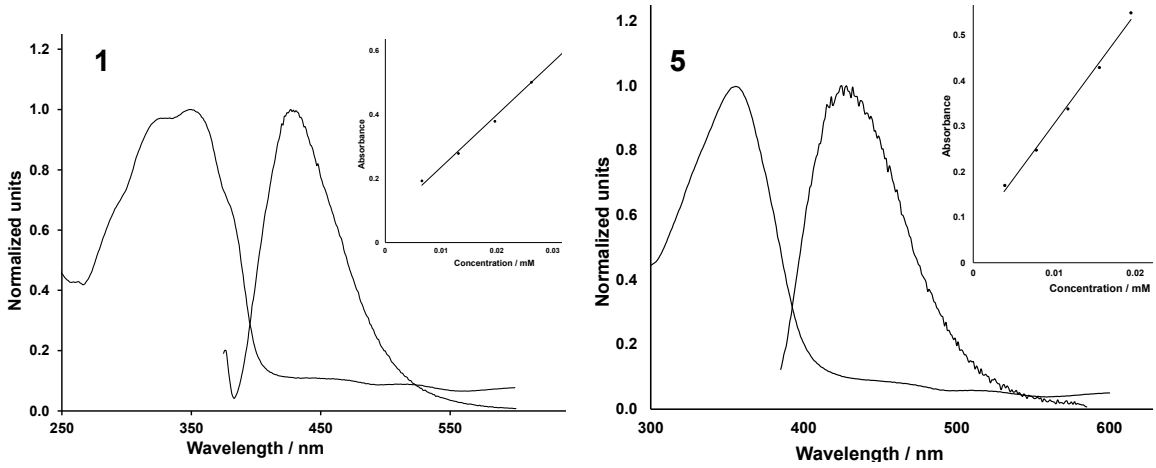


Figure 7. Graphical overlay of compound **2** coloured green and **6** coloured red. The RMS value is 0.173 Å. O1, O2, C1, C2, and C3 were used to calculate the overlay in MERCURY [34].

2.3. Spectroscopy

UV/vis absorbance and fluorescence spectra were measured as a characterization method for compounds **1–8** in ethanol solutions with concentrations varying from 2 to 10 ppm. Representative UV/vis absorbance and fluorescence spectra of ligand **1** and rhodium(I) complex **5** are shown in Figure 8, with other spectra available in supplementary information. Spectroscopic data for all compounds are summarized in Table 5. The absorbance spectra showed a wide absorbance peak, with maxima between 350 and 370 nm for β-diketonato ligands and rhodium(I) complexes. This peak is usually attributed to the π–π* transition in the fluorene group [35]. Absorbance sub-peaks were also observed between 450 and 600 nm. These peaks are listed in Table 5. Minimal shifts in absorbance maxima were observed for rhodium(I) complexes **5–8**, when compared to their corresponding free ligands. This indicates that electron-withdrawing or donating groups on the β-diketonato phenyl group has little influence on the electronic properties of the metal complexes. Compounds **1** and **5**, containing a CF_3 group on the β-diketonato backbone showed absorbance maxima at a significantly lower wavelength as a result of the electron-withdrawing effect of the CF_3 group directly on the ligand backbone. Fluorescence spectra were measured by excitation at 350 nm for compounds **1** and **5**, and excitation at 370 nm for all other compounds. All compounds exhibited fluorescent properties; however, intensities were

quite low under our experimental conditions. Quantum yields are not reported, since values determined against anthracene as standard were found to be less than 0.1%.



(**a**) (**b**)

Figure 8. Spectra of β-diketonato ligand, 1 (**a**) and rhodium complex, 5 (**b**), showing UV/vis and fluorescence. Fluorescence spectra were obtained by excitation at 350 nm. The insert shows UV/vis absorbance vs. concentration, used to validate the Beer–Lambert law. Absorbance and fluorescence were measured in ethanol at concentrations of 2–10 ppm.

Table 5. UV/vis spectroscopy data for compounds **1**–**8**.

Compound	λ_{max} (nm)	ε ($M^{-1}cm^{-1}$)	λ_{max} (nm)	Compound	λ_{max} (nm)	ε ($M^{-1}cm^{-1}$)	λ_{max} (nm)
1	349	16,383	458, 516	**5**	357	24,151	460, 517
2	370	31,030	457, 518	**6**	366	16,643	457, 514
3	366	39,448	455, 515	**7**	362	21,319	454, 514
4	369	32,462	456, 514	**8**	366	17,047	455, 513

2.4. Electrochemistry

Cyclic voltammetry (CV) of compounds **1–8** was measured in acetonitrile and tetra-*n*-butylammonium hexafluorophosphate [^{n}Bu$_4$N][PF$_6$] as a solvent and supporting electrolyte system. This solvent and electrolyte system has previously been used for several similar rhodium(I) complexes [18,22,36]. Utilizing this solvent and electrolyte system enables us to compare our results with similar compounds with varying size and electronic properties.

CVs of all β-diketones used, **1**–**4**, are shown in Figure 9, and the most notable electrochemical parameters are listed in Table 6. The electrochemical activity only shows one reduction wave between −1500 mV and −2100 mV, as measured against ferrocene (FcH) as the internal standard. This reduction wave is a result of reduction on the β-diketonato backbone, as previously reported [18,36]. The substituents on the ligand backbone have a significant influence on the position of this reduction wave. Electron-rich substituents donate electron density to the ligand-backbone system, making it more electron-rich and, as a result, more difficult to reduce. This moves the reduction wave to a lower potential. It is thus expected that the β-diketone ligand containing an electron-withdrawing CF_3 group (**1**) will be reduced at the highest potential (−1480 mV). The reduction potential of the other phenyl-containing β-diketones decreases in the order of increased electron density of the phenyl-containing group, i.e., $PhCF_3$ (**2**), Ph (**3**) and $PhCH_3$ (**4**). The reduction wave was found to be electrochemically quasi-reversible with ΔEp values between 100 and 140 mV. This wave was also found to be chemically irreversible, with i_{pa}/i_{pc} values of

approximately 0.5. This is expected, since the product of reduction is an unstable radical species, which quickly decomposes before oxidation is possible on the reverse scan [36]. Since the β-diketone can exist in either the keto or enol form, it is possible to observe both distinctly on a CV [22]. This, however, was not the case in this study, and only one reduction wave representing the enol form was observed. This is in correlation with NMR and crystallographic observations that the β-diketones in this study mainly exist in the enol form.

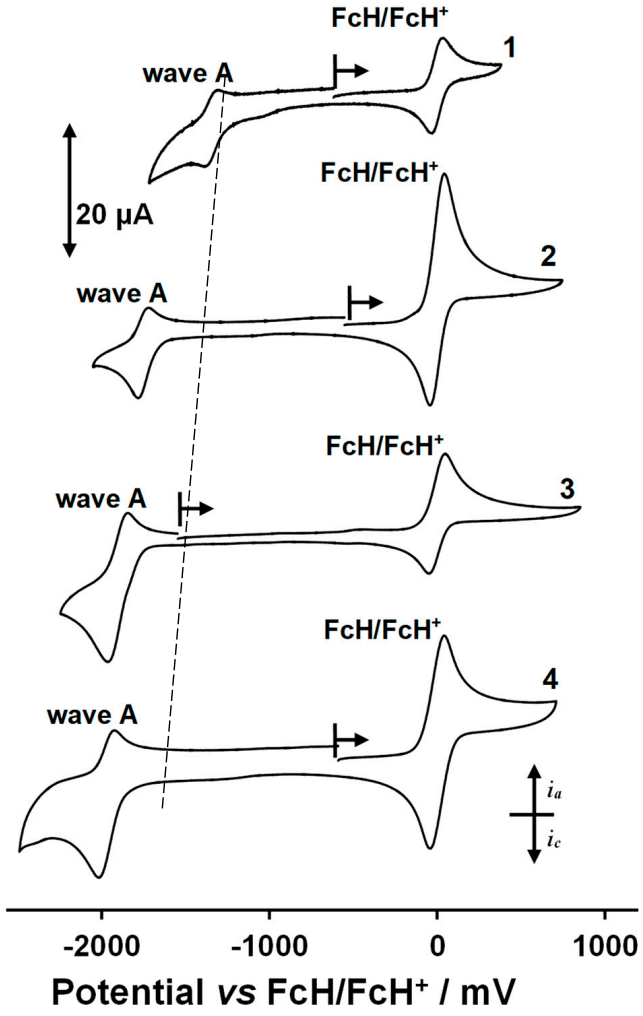


Figure 9. CVs measured at 100 mV/s of β-diketones **1**–**4** in CH_3CN and $[^nBu_4N][PF_6]$ as solvent and supporting electrolyte. Scans were measured at 25 °C, and ferrocene (FcH) was used as an internal standard.

CVs of rhodium(I) β-diketonato complexes **5**–**8** are shown in Figure 10, and selected electrochemical parameters are listed in Table 6. Electrochemical measurements were performed with decamethyl ferrocene (Fc^*) as an internal standard, since ferrocene could not be used due to interference with wave B. Decamethyl ferrocene was referenced against ferrocene under current conditions in a separate experiment. The electrochemical activity shows the oxidation wave B of the rhodium(I) centre, as well as the reduction wave A based on the β-diketonato ligand backbone, similar to that observed for **1**–**4**. The reduction wave A of the β-diketonato backbone is observed below −2000 mV for **6**–**8** and at −1880 mV for **5**. This indicates a clear shift towards a lower potential, as a result of complexation to the metal centre. Complexation to the metal centre, increases the electron density on the ligand backbone, making it more difficult to reduce, thus lowering the

reduction potential. Complexation to the metal centre also increases the electrochemical reversibility (ΔE_p < 90 mV) of wave A. Oxidation of the metal centre is observed at wave B at approximately. 300 mV. This is in accordance with previous reports of rhodium(I) oxidation [18,37]. No clear trend was observed in the electronic influence of β-diketonato ligand substitution on the ease of oxidation of the metal centre. This is expected, since the variation mostly exists on the phenol ring (Ph, $PhCH_3$ or $PhCF_3$) of the ligand. The phenol ring is three bonds away from the metal centre, while the varied substituent is on the para-position, making the distance to the metal centre too far to have any noticeable influence on the electronic properties of the metal centre. The oxidation of the rhodium(I) centre is a two-electron oxidation process to form a rhodium(III) species. It is possible for rhodium(I) to form either a rhodium(II) or rhodium(III) species upon oxidation, but this has been shown to be highly dependent on the solvent and supporting electrolyte system chosen [38]. When a non-coordinating electrolyte and solvent system is chosen, a rhodium(II) species is formed, which is unstable and decomposes quickly [39,40]. A solvent and electrolyte system that can coordinate leads to the formation of a rhodium(III) species. The vacant coordination sites of the octahedral rhodium(III) species are filled by the coordinating solvent, in this case acetonitrile [41]. This octahedral rhodium(III) species is oxidised, usually at a potential around −1300 mV [37]. In this study, some reversible Rh(III) reduction is observed between 200 and 300 mV, as well as some solvent-coordinated Rh(III) reduction between −1300 and −1500 mV. However, since this coordinated species diffuses away from the surface of the electrode before the reverse scan reaches this potential, this peak was too small to be quantified.

Table 6. Electrochemical values obtained for compounds **1** – **8**, measured at 100 mV/s and 25 °C. CVs were measured in CH_3CN and $[^nBu_4N][PF_6]$ as supporting electrolyte.

Compound	Wave	E_{pa} (mV)	i_{pa} (μA)	ΔE_p (mV)	$E^{\circ\prime}$ (mV)	i_{pc}/i_{pa}
1	A	−1480 *	4.6 *	140	−1410	0.80 *
2	A	−1835 *	7.3 *	104	−1783	0.51 *
3	A	−2019 *	12.8 *	132	−1953	0.49 *
4	A	−2058 *	12.5 *	137	−1989	0.47 *
5	A	−1886 *	2.8 *	82	−1845	0.82 *
	B	361	3.1	122	300	0.29
6	A	−2073 *	3.1 *	103	−2022	0.49 *
	B	536	1.3	105	483	0.61
7	A	−2129 *	2.3 *	89	−2084	0.78 *
	B	286	1.7	142	215	0.47
8	A	−2000 *	3.2 *	88	−1956	0.28 *
	B	326	1.2	130	315	0.42

*, E_{pc}, i_{pc} and i_{pa}/i_{pc} for reduction waves A.

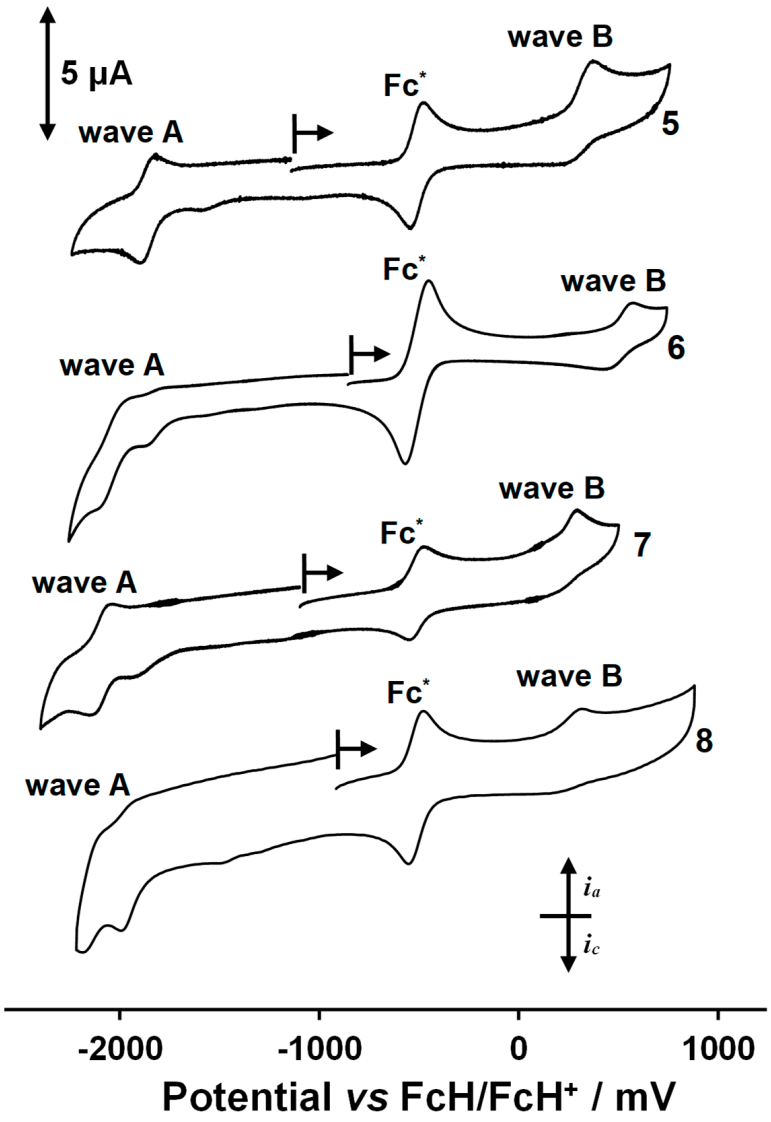


Figure 10. CVs of rhodium(I) complexes **5–8** measured at 100 mV/s, in CH_3CN and $[^nBu_4N][PF_6]$ as solvent and supporting electrolyte. Scans were measured at 25 °C. Decamethyl ferrocene (Fc^*) was used as an internal standard.

3. Materials and Methods

3.1. General

Chemicals were used as purchased from Merck chemical company, without further purification. Tetrahydrofuran (THF) was dried over sodium and distilled before use. A 600 MHz AVANCE II NMR spectrometer (Bruker, Johannesburg, South Africa), operating at 25 °C, was used to collect ^1H NMR and ^{13}C NMR spectra. TMS was used as an internal reference for the determination of chemical shifts (δ ppm). J values are given in Hz. UV/vis absorbance spectra were measured on a Cary 60 spectrophotometer (JLW Supplies, Cape Town, South Africa), and fluorescence measurements were carried out on a Cary Eclipse spectrophotometer (JLW Supplies, Cape Town, South Africa). A quartz cuvette with 1 cm path length was used for absorbance and fluorescence measurements of 10 to 2 ppm solutions in spectroscopic grade ethanol of **1–8**. Fluorescence intensity was found to be low, and quantum yields were not determined. A Bruker Tensor 27 instrument (Bruker, Johannesburg, South Africa) with an ATR attachment was used to record FTIR spectra. Chromatography was performed on silica (230–400 mesh).

3.2. Synthesis

3.2.1. β-Diketone Syntheses

β-diketonato ligands were synthesized according to a previously reported method [18].

Compound **1**:

Acetyl fluorene (1.00 g, 4.80 mmol), ethyl trifluoroacetate (0.69 mL, 0.824 g, 5.8 mmol). RF = 0.54 (hexane:ether: 1:1). Yield −19% (0.28 g). ^{1}H NMR (600 MHz, $CDCl_3$, 25 °C): 8.15 (1H, s, ArH), 8.01 (1H, d, ArH), 7.88 (2H, t, ArH), 7.61 (1H, d, ArH), 7.43 (2H, m, ArH), 6.64 (1H, s, CH methine), 3.99 (2H, s, CH_2 cp ring), ppm; ^{13}C NMR (600 MHz, $CDCl_3$, 25 °C): 186.44 (carbonyl), 176.83 (enol), 147.84 (aromatic), 144.59 (aromatic), 143.76 (aromatic), 140.20 (aromatic), 131.03 (aromatic), 128.60 (aromatic), 127.27 (aromatic), 127.08 (aromatic), 125.37 (aromatic), 124.33 (aromatic), 121.12 (aromatic), 120.19 (aromatic), 92.22 (methine), 36.90 (methylene), 29.71 (CF_3) ppm. IR: υ(C-O) = 1584, 1563 cm^{-1}.

Compound **2**:

Acetyl fluorene (1.00 g, 4.80 mmol), methyl 4-(trifluoromethyl)benzoate (0.93 mL, 1.18 g, 5.8 mmol). RF = 0.70 (hexane:ether: 1:1). Yield −16% (0.35 g). ^{1}H NMR (600 MHz, CDCl3, 25 °C): 8.29 (1H, s, ArH), 8.11 (2H, d Ph), 8.05 (1H, d, ArH), 7.89 (1H, d, ArH), 7.87 (1H, d, ArH), 7.74 (2H, d, Ph), 7.61 (1H, d, ArH), 7.44 (1H, t, ArH), 7.39 (1H, t, ArH), 6.94 (1H, s, CH methine), 4.00 (2H, s, CH_2 cp ring), ppm; ^{13}C NMR (600 MHz, CDCl3, 25 °C): 187.33 (carbonyl), 182.79 (enol), 146.57 (aromatic), 144.43 (aromatic), 143.61 (aromatic), 140.54 (aromatic), 138.87 (aromatic), 133.60 (aromatic), 128.16 (aromatic), 127.43 (aromatic), 127.16 (aromatic), 126.65 (aromatic), 125.70 (aromatic), 125.68 (aromatic), 125.32 (aromatic), 124.06 (aromatic), 120.90 (aromatic), 119.98 (aromatic),93.72 (methine), 36.96 (methylene), 30.36 (cod), 25.66 (CF_3) ppm. IR: υ(C-O) = 1609, 1586 cm^{-1}.

Compound **3**:

Acetyl fluorene (1.00 g, 4.80 mmol), methyl benzoate (0.72 mL, 0.79 g, 5.8 mmol). RF = 0.56 (hexane:ether: 1:1). Yield −21% (0.38 g). ^{1}H NMR (600 MHz, $CDCl_3$, 25 °C): 8.19 (1H, s, ArH), 8.04 (1H, d, ArH), 8.01 (2H, d Ph), 7.86 (2H, t, ArH), 7.60 (1H, d, ArH), 7.56 (1H, t, Ph), 7.50 (2H, t, Ph), 7.43 (1H, t, ArH), 7.38 (1H, t, ArH), 6.93 (1H, s, CH methine), 3.99 (2H, s, CH_2 cp ring), ppm; ^{13}C NMR (600 MHz, $CDCl_3$, 25 °C): 186.15 (carbonyl), 185.19 (enol), 146.10 (aromatic), 144.37 (aromatic), 143.51 (aromatic), 140.64 (aromatic), 135.66 (aromatic), 133.88 (aromatic), 132.36 (aromatic), 128.69 (aromatic), 127.98 (aromatic), 127.16 (aromatic), 127.09 (aromatic), 126.43 (aromatic), 125.28 (aromatic), 123.90 (aromatic), 120.80 (aromatic), 119.89 (aromatic), 93.15 (methine), 36.94 (methylene) ppm. IR: υ(C-O) = 1596, 1587 cm^{-1}.

Compound **4**:

Acetyl fluorene (1.00 g, 4.80 mmol), ethyl 4-methylbenzoate (0.93 mL, 0.95 g, 5.8 mmol). RF = 0.63 (hexane:ether: 1:1). Yield −18% (0.34 g). ^{1}H NMR (600 MHz, $CDCl_3$, 25 °C): 8.18 (1H, s, ArH), 8.03 (1H, d, ArH), 7.93 (2H, d Ph), 7.86 (2H, t, ArH), 7.59 (1H, d, ArH), 7.42 (1H, t, ArH), 7.38 (1H, t, ArH), 7.30 (2H, d, Ph), 6.90 (1H, s, CH methine), 3.99 (2H, s, CH_2 cp ring), 2.44 (3H, s, CH3) ppm; ^{13}C NMR (600 MHz, $CDCl_3$, 25 °C): 185.61 (carbonyl), 185.54 (enol), 145.98 (aromatic), 144.36 (aromatic), 143.51 (aromatic), 140.71 (aromatic), 134.02 (aromatic), 133.00 (aromatic), 129.43 (aromatic), 127.94 (aromatic), 127.24 (aromatic), 127.09 (aromatic), 126.38 (aromatic), 125.29 (aromatic), 123.85 (aromatic), 120.78 (aromatic), 119.89 (aromatic), 92.84 (methine), 36.97 (methylene), 25.64 (methyl) ppm. IR: υ(C-O) = 1604, 1582 cm^{-1}.

3.2.2. Rh Complexation

Rh complexes containing β-diketonato ligands were synthesized as previously discussed [18].

Compound **5**:

$[Rh_2Cl_2(cod)_2]$ (0.015 g, 0.03 mmol), compound **1** (0.020 g, 0.06 mmol). Yield −89% (0.027 g). ^{1}H NMR (600 MHz, $CDCl_3$, 25 °C): 7.97 (1H, s, ArH), 7.84 (2H, m, ArH), 7.77 (1H, d, ArH), 7.58 (1H, d, ArH), 7.39 (2H, m, ArH), 6.48 (1H, s, CH methine), 4.30 (4H, d, cod), 3.94 (2H, s, CH_2 cp ring), 2.53 (4H, m, cod), 1.92 (4H, m, cod), ppm; ^{13}C NMR (600 MHz, $CDCl_3$, 25 °C): 185.59 (carbonyl), 169.91 (carbonyl), 145.86 (aromatic), 144.36 (aromatic), 143.35 (aromatic), 140.63 (aromatic), 136.12 (aromatic), 127.91 (aromatic), 127.07 (aromatic), 126.96 (aromatic), 125.26 (aromatic), 124.34 (aromatic), 120.76 (aromatic), 119.73 (aromatic), 91.80 (methine), 77.75 (cod), 77.65 (cod), 77.32 (cod), 36.91 (methylene), 30.33 (cod), 30.27 (cod), 30.25 (cod), 29.71 (CF_3) ppm. IR: υ(C-O) = 1564 cm^{-1}.

Compound **6**:

$[Rh_2Cl_2(cod)_2]$ (0.015 g, 0.03 mmol), compound **2** (0.020 g, 0.06 mmol). Yield −82% (0.029 g). ^{1}H NMR (600 MHz, $CDCl_3$, 25 °C): 8.01 (1H, s, ArH), 7.94 (2H, d, Ph), 7.88 (1H, d, ArH), 7.83 (1H, d, ArH), 7.78 (1H, d, ArH), 7.65 (2H, d, Ph), 7.57 (1H, d, ArH), 7.40 (1H, t, ArH), 7.35 (1H, t, ArH), 6.71 (1H, s, CH methine), 4.32 (4H, d, cod), 3.94 (2H, s, CH_2 cp ring), 2.56 (4H, m, cod), 1.94 (4H, d, cod) ppm; ^{13}C NMR (600 MHz, $CDCl_3$, 25 °C): 182.45 (carbonyl), 179.43 (enol), 144.80 (aromatic), 144.20 (aromatic), 143.29 (aromatic), 143.24 (aromatic), 140.91 (aromatic), 137.68 (aromatic), 127.60 (aromatic), 127.57 (aromatic), 126.99 (aromatic), 125.21 (aromatic), 124.09 (aromatic), 120.56 (aromatic), 119.57 (aromatic), 94.52 (methine), 77.33 (cod), 77.32 (cod), 36.95 (methylene), 30.36 22.67 (t, CF_3) ppm. IR: υ(C-O) = 1579 cm^{-1}.

Compound **7**:

$[Rh_2Cl_2(cod)_2]$ (0.015 g, 0.03 mmol), compound **3** (0.020 g, 0.06 mmol). Yield −84% (0.026 g). ^{1}H NMR (600 MHz, $CDCl_3$, 25 °C): 8.01 (1H, s, ArH), 7.89 (1H, d, ArH), 7.85 (2H, d Ph), 7.82 (1H, d, ArH), 7.76 (1H, d, ArH), 7.56 (1H, d ArH), 7.45 (1H, t, ArH), 7.39 (3H, t, Ph), 7.34 (1H, t, ArH), 6.73 (1H, s, CH methine), 4.31 (4H, d, cod), 3.94 (2H, s, CH_2 cp ring), 2.56 (4H, m, cod), 1.93 (4H, d, cod), ppm; ^{13}C NMR (600 MHz, $CDCl_3$, 25 °C): 181.56 (carbonyl), 181.27 (carbonyl), 144.43 (aromatic), 144.16 (aromatic), 143.15 (aromatic), 141.04 (aromatic), 139.86 (aromatic), 138.12 (aromatic), 130.71 (aromatic), 128.23 (aromatic), 127.40 (aromatic), 127.34 (aromatic), 126.92 (aromatic), 126.49 (aromatic), 125.17 (aromatic), 124.04 (aromatic), 120.47 (aromatic), 119.48 (aromatic), 94.13 (methine), 78.75 (cod), 78.65 (cod), 36.95 (methylene), 30.89 (cod), 30.38 (cod), 29.71 (cod) ppm. IR: υ(C-O) = 1584 cm^{-1}.

Compound **8**:

$[Rh_2Cl_2(cod)_2]$ (0.015 g, 0.03 mmol), compound **4** (0.020 g, 0.06 mmol). Yield −87% (0.027 g). ^{1}H NMR (600 MHz, $CDCl_3$, 25 °C): 8.00 (2H, d, Ph), 7.88 (1H, d, ArH), 7.82 (1H, d, ArH), 7.76 (3H, d, ArH, Ph), 7.57 (1H, d, ArH), 7.39 (1H, t, ArH), 7.34 (1H, t, ArH), 7.19 (2H, d, Ph), 6.71 (1H, s, CH methine), 4.29 (4H, d, cod) 3.94 (2H, s, CH_2 cp ring), 2.55 (4H, m, cod), 2.17 (3H, s, CH3), 1.93 (4H, d, cod), ppm; ^{13}C NMR (600 MHz, $CDCl_3$, 25 °C): 181.26 (carbonyl), 181.24 (carbonyl), 144.33 (aromatic), 144.17 (aromatic), 143.14 (aromatic), 141.18 (aromatic), 141.08 (aromatic), 138.27 (aromatic), 137.01 (aromatic), 128.97 (aromatic), 127.39 (aromatic), 126.93 (aromatic), 126.47 (aromatic), 125.19 (aromatic), 124.04 (aromatic), 120.48 (aromatic), 119.47 (aromatic), 93.86 (methine), 76.94 (cod), 68.01 (cod), 36.97 (methylene), 30.96 (cod), 30.40 (cod), 29.73 (cod), 25.64 (methyl) ppm. IR: υ(C-O) = 1581 cm^{-1}.

3.3. X-Ray Structure Determination and Refinement of **2** *and* **6**

The reflection data were collected on a Bruker D8 Venture 4K Kappa Photon III C28 diffractometer. The diffractometer was equipped with a graphite monochromator using a Cu-Kα X-ray generator with a wavelength of λ = 1.54178 Å. Data were collected utilizing both phi and omega scans at a temperature of 100 K. COSMO [42] was utilized for multiple hemisphere data collection of the reciprocal space. Bruker SAINT-Plus and XPREP [43] were employed for frame integration and data reduction, respectively. SADABS [44] was used for

phase correction through the multi-scan method. SHELXT [45] was used to solve the crystal structures through intrinsic phasing. Olex2 [46] and SHELXL-2018/3 [45] were used for the refinement of the crystal structures. DIAMOND 4.0 [24] and MERCURY [34] were utilized for image generation. Thermal ellipsoids are drawn with a 50% probability level if not stated otherwise. In all structures, the hydrogen atoms were positioned geometrically and refined using a riding model: C-H aromatic distances at 0.95Å; and methylene C-H distances at 0.99 Å. The H atom isotropic displacement parameters were fixed at $U_{iso}(H) = 1.2\ U_{eq}(C)$. The hydrogen atoms bound to non-carbon atoms were located and placed according to the Fourier electron density difference map. In each image, the hydrogen labels have been removed for the sake of clarity unless used to indicate hydrogen bonding.

3.4. Electrochemistry of **1**–**8**

Electrochemical measurements were carried out using 0.5 mM solutions of **1**–**8** in acetonitrile containing 0.10 M tetrabutylammonium hexafluorophosphate, $[N(^nBu)_4][PF_6]$, as supporting electrolyte. Experiments were performed under argon at 25 °C utilizing a BAS 100 B/W electrochemical potentiostat. A three-electrode cell setup was used, consisting of a Pt auxiliary electrode, a glassy carbon working electrode (surface area 0.0707 cm^2), and a Pt wire reference electrode. Successive experiments were reproducible within 5 mV. Results are reported as referenced against the ferrocene/ferrocenium (FcH/FcH^+) couple at 0 V as suggested by IUPAC [47]. Ferrocene was used as an internal standard for compounds **1**–**4**, while decamethyl ferrocene (Fc^*) was employed as an internal standard for compounds **5**–**8**. Experiments were first performed in the absence of ferrocene or decamethyl ferrocene and repeated in the presence of <0.5 mM of the internal standard. A separate experiment containing only ferrocene and decamethyl ferrocene was also performed. Data were then adjusted to set the formal reduction potential of FcH/FcH^+ to 0 V. Under our conditions, the Fc^*/Fc^{*+} couple was at −515 mV vs. FcH/FcH^+.

4. Conclusions

The synthesis of four fluorene-containing β-diketone ligands is discussed, where the varying substituents were CF_3 (**1**), $PhCF_3$ (**2**), Ph (**3**) and $PhCH_3$ (**4**). These were also used to synthesize the corresponding cyclooctadiene rhodium(I) complexes of the type [Rh(cod)((fluorene)COCHCOR)], with R = CF_3 (**5**), $PhCF_3$ (**6**), Ph (**7**) and $PhCH_3$ (**8**). A crystal structure determination of **2** and **6** was performed. This showed a hydrogen interaction between the hydroxy and carboxyl groups of the β-diketone structure, forming a pseudo six-membered ring that stabilizes the dominant enol form of the compound. Comparing the crystal structure of ligand **2** to that of metal complex **6**, we observed geometric stress on the ligand and out-of-plane bending, as a result of coordination with the metal. Electrochemical analysis of the β-diketones **1**–**4** showed the influence of the varying R group on the reducing potential of the ligand backbone, while the influence on that of the rhodium(I) complex was negligible.

Supplementary Materials: The following supporting information can be downloaded at: https://www.mdpi.com/article/10.3390/inorganics13080255/s1, All ^1H and ^{13}C NMR spectra, as well as UV/vis and fluorescence spectra of all compounds.

Author Contributions: Conceptualization and methodology, E.F.; validation, F.J.F.J. and E.F.; formal analysis, S.K., F.J.F.J. and E.F.; investigation, S.K., F.J.F.J. and E.F.; resources, F.J.F.J. and E.F.; data curation, F.J.F.J. and E.F.; writing—original draft preparation, F.J.F.J. and E.F.; writing—review and editing, F.J.F.J. and E.F.; visualization, F.J.F.J. and E.F.; supervision, E.F.; project administration, E.F.; funding acquisition, E.F. All authors have read and agreed to the published version of the manuscript.

Funding: This research was funded by the Central Research Fund of the UFS and the APC was funded by the Library and Information Services of the UFS.

Institutional Review Board Statement: Not applicable.

Informed Consent Statement: Not applicable.

Data Availability Statement: Data is contained within the article or Supplementary Materials available; any additional data is available on request from the authors.

Conflicts of Interest: The authors declare no conflicts of interest.

Abbreviations

The following abbreviations are used in this manuscript:

cod	cyclooctadiene
LDA	Lithium diisopropylamine
NMR	Nuclear magnetic resonance
FTIR	Fourier transform infrared
CSD	Cambridge structural database
CV	Cyclic voltammetry
FcH	Ferrocene
Fc^*	Decamethylferrocene
THF	tetrahydrofuran

References

1. Shaya, J.; Corridon, P.R.; Al-Omari, B.; Aoudi, A.; Shunnar, A.; Mohideen, M.I.H.; Qurashi, A.; Michel, B.Y.; Burger, A. Design, photophysical properties, and applications of fluorene-based fluorophores in two-photon fluorescence bioimaging: A review. *J. Photochem. Photobiol. C Photochem. Rev.* **2022**, *52*, 100529. [CrossRef]
2. Liu, J.-W.; Zhou, H.-C.; Wang, Z.-K.; Tang, X.; Wu, H.-Y.; Wang, S.; Lai, W.-Y.; Li, Y.-H. Distinct Ir(III) complexes containing unsymmetric ligands with fluorene-oxadiazole groups and their performance of organic light-emitting diodes. *Dye. Pigment.* **2022**, *202*, 110252. [CrossRef]
3. Tahir Waseem, M.; Muhammad Junaid, H.; Gul, H.; Ali Khan, Z.; Yu, C.; Anjum Shahzad, S. Fluorene based fluorescent and colorimetric sensors for ultrasensitive detection of nitroaromatics in aqueous medium. *J. Photochem. Photobiol. A Chem.* **2022**, *425*, 113660. [CrossRef]
4. Bezgin Carbas, B. Fluorene based electrochromic conjugated polymers: A review. *Polymer* **2022**, *254*, 125040. [CrossRef]
5. Li, H.; Yu, M.; Luo, M.; Li, Y.; Chen, Z.; He, J.; Wu, M.; Liu, Y.; Wang, K.; Zhan, X.; et al. Reconfigurable amplified circularly polarized photo/electro-luminescence from simple solution self-assembly of a chiral deep-blue fluorene-based conjugated polymer. *J. Mater. Chem. C* **2025**, *13*, 13731–13741. [CrossRef]
6. Zhu, S.; Pan, Q.; Li, Y.; Liu, W.; Liu, R.; Zhu, H. Fluorene-decorated Ir(iii) complexes: Synthesis, photophysics and tunable triplet excited state properties in aggregation. *Dalton Trans.* **2022**, *51*, 13322–13330. [CrossRef]
7. Pham, H.D.; Gil-Escrig, L.; Feron, K.; Manzhos, S.; Albrecht, S.; Bolink, H.J.; Sonar, P. Boosting inverted perovskite solar cell performance by using 9,9-bis(4-diphenylaminophenyl)fluorene functionalized with triphenylamine as a dopant-free hole transporting material. *J. Mater. Chem. A* **2019**, *7*, 12507–12517. [CrossRef]
8. Zuo, X.; Zhang, S.; Bai, H.; Yu, Q.; Zhao, Q.; Sun, M.; Zhao, X.; Feng, X. Effects of fluorene-9-bisphenol exposure on anxiety-like and social behavior in mice and protective potential of exogenous melatonin. *Environ. Sci. Pollut. Res.* **2024**, *31*, 29385–29399. [CrossRef] [PubMed]
9. Hussein, E.M.; Alsantali, R.I.; Morad, M.; Obaid, R.J.; Altass, H.M.; Sayqal, A.; Abourehab, M.A.S.; Elkhawaga, A.A.; Aboraia, A.S.M.; Ahmed, S.A. Bioactive fluorenes. Part III: 2,7-dichloro-9H-fluorene-based thiazolidinone and azetidinone analogues as anticancer and antimicrobial against multidrug resistant strains agents. *BMC Chem.* **2020**, *14*, 42. [CrossRef]
10. Urade, R.; Chang, W.-T.; Ko, C.-C.; Li, R.-N.; Yang, H.-M.; Chen, H.-Y.; Huang, L.-Y.; Chang, M.-Y.; Wu, C.-Y.; Chiu, C.-C. A fluorene derivative inhibits human hepatocellular carcinoma cells by ROS-mediated apoptosis, anoikis and autophagy. *Life Sci.* **2023**, *329*, 121835. [CrossRef]
11. Feng, Q.; Liu, Y.; Zou, L.; Lei, M.; Zhu, C.; Xia, W. Fluorene-9-bisphenol exposure damages the testis in mice through a novel mechanism of ferroptosis. *Food Chem. Toxicol.* **2024**, *184*, 114385. [CrossRef]

12. Kumbar, M.; Patil, S.A.; Toragalmath, S.S.; Jawoor, S.S.; Shettar, A. Synthesis of novel metal (II) complexes tailored from 9-oxo-9H-fluorene-1-carboxylic acid via green protocol: DNA cleavage and anticancer studies. *Inorganica Chim. Acta* **2020**, *500*, 119210. [CrossRef]
13. Marufa, S.S.; Rahman, T.; Rahman, M.M.; Rahman, M.M.; Khan, S.J.; Jahan, R.; Nishino, H.; Alam, M.S.; Haque, M.A. Design, synthesis, molecular docking, and dynamics studies of novel thiazole-Schiff base derivatives containing a fluorene moiety and the assessment of their antimicrobial and antioxidant activity. *RSC Adv.* **2024**, *14*, 35198–35214. [CrossRef]
14. Haghdoost, M.M.; Golbaghi, G.; Guard, J.; Sielanczyk, S.; Patten, S.A.; Castonguay, A. Synthesis, characterization and biological evaluation of cationic organoruthenium(ii) fluorene complexes: Influence of the nature of the counteranion. *Dalton Trans.* **2019**, *48*, 13396–13405. [CrossRef]
15. Popa, A.D.; Mădălan, A.M. Silver(I) complexes with a luminescent tripodal Schiff base ligand derived from fluorene-2-carboxaldehyde. *Polyhedron* **2022**, *220*, 115849. [CrossRef]
16. Zhao, Z.; Han, X.; Liu, K.; Zhao, L.; Liu, Q. Six Fluorene-Based N-Heterocyclic Carbene Silver(I) Complexes: Structural Study and Recognition for $Cu2^{+}$. *Organometallics* **2022**, *41*, 2394–2405. [CrossRef]
17. Tian, Z.; Yang, X.; Liu, B.; Zhong, D.; Zhou, G. Photophysical properties and optical power limiting ability of Pt(II) polyynes bearing fluorene-type ligands with ethynyl units at different positions. *J. Organomet. Chem.* **2019**, *895*, 28–36. [CrossRef]
18. Fourie, E. Fluorene-containing β-diketonato ligands and their Rhodium(I) complexes. *Inorganica Chim. Acta* **2021**, *517*, 120209. [CrossRef]
19. de Gonzalo, G.; Alcántara, A.R. Recent Developments in the Synthesis of β-Diketones. *Pharmaceuticals* **2021**, *14*, 1043. [CrossRef]
20. Woodward, A.W.; Frazer, A.; Morales, A.R.; Yu, J.; Moore, A.F.; Campiglia, A.D.; Jucov, E.V.; Timofeeva, T.V.; Belfield, K.D. Two-photon sensitized visible and near-IR luminescence of lanthanide complexes using a fluorene-based donor–π-acceptor diketonate. *Dalton Trans.* **2014**, *43*, 16626–16639. [CrossRef]
21. Suwa, Y.; Yamaji, M.; Okamoto, H. Synthesis and photophysical properties of difluoroboronated β-diketones with the fluorene moiety that have high fluorescence quantum yields. *Tetrahedron Lett.* **2016**, *57*, 1695–1698. [CrossRef]
22. Kemp, K.C.; Fourie, E.; Conradie, J.; Swarts, J.C. Ruthenocene-Containing β-Diketones: Synthesis, pKa′ Values, Keto–Enol Isomerization Kinetics, and Electrochemical Aspects. *Organometallics* **2008**, *27*, 353–362. [CrossRef]
23. Conradie, J.; Lamprecht, G.J.; Otto, S.; Swarts, J.C. Synthesis and characterisation of ferrocene-containing β-diketonato complexes of rhodium(I) and rhodium(III). *Inorganica Chim. Acta* **2002**, *328*, 191–203. [CrossRef]
24. Brandenburg, K.; Putz, H. *Diamond*, version 4.0; 53002; Crystal Impact GbR: Bonn, Germany, 2005.
25. Wang, Q.; Bian, Y.; Dhawan, G.; Zhang, W.; Sorochinsky, A.E.; Makarem, A.; Soloshonok, V.A.; Han, J. FDA approved fluorine-containing drugs in 2023. *Chin. Chem. Lett.* **2024**, *35*, 109780. [CrossRef]
26. Groom, C.R.; Bruno, I.J.; Lightfoot, M.P.; Ward, S.C. The Cambridge Structural Database. *Acta Crystallogr. Sect. B* **2016**, *72*, 171–179. [CrossRef]
27. Wu, K.; Zhang, T.; Wang, Z.; Wang, L.; Zhan, L.; Gong, S.; Zhong, C.; Lu, Z.-H.; Zhang, S.; Yang, C. De Novo Design of Excited-State Intramolecular Proton Transfer Emitters via a Thermally Activated Delayed Fluorescence Channel. *J. Am. Chem. Soc.* **2018**, *140*, 8877–8886. [CrossRef] [PubMed]
28. Dalal, A.; Kamboj, R.C.; Kumar, D.; Sharma, M.K.; Selvarajan, N. Crystal structure of (Z)-3-[5-chloro-2-(prop-2-ynyloxy)phenyl]-3-hydroxy-1-[4-(trifluoromethyl)phenyl]prop-2-en-1-one. *Acta Crystallogr. Sect. E* **2015**, *71*, o556–o557. [CrossRef]
29. Sato, K.; Sandford, G.; Shimizu, K.; Akiyama, S.; Lancashire, M.J.; Yufit, D.S.; Tarui, A.; Omote, M.; Kumadaki, I.; Harusawa, S.; et al. Synthesis of fluorinated isoxazoles using Selectfluor™: Preparation and characterization of 4-fluoroisoxazole, 4,4,5-trifluoroisoxazoline and 4,4-difluoro-5-hydroxyisoxazoline systems from one-pot and multi-step processes. *Tetrahedron* **2016**, *72*, 1690–1698. [CrossRef]
30. Butler, T.; Mathew, A.S.; Sabat, M.; Fraser, C.L. Camera Method for Monitoring a Mechanochromic Luminescent β-Diketone Dye with Rapid Recovery. *ACS Appl. Mater. Interfaces* **2017**, *9*, 17603–17612. [CrossRef]
31. Jecny, J.; Huml, K. The crystal and molecular structure of 1,3-diphenyl-1,3-propanedione-(1,6-dichloro-1,5-cyclooctadiene)rhodium(I). *Acta Crystallogr. Sect. B* **1974**, *30*, 1105–1110. [CrossRef]
32. Mang, A.; Rotthowe, N.; Beltako, K.; Linseis, M.; Pauly, F.; Winter, R.F. Single-molecule conductance studies on quasi- and metallaaromatic dibenzoylmethane coordination compounds and their aromatic analogs. *Nanoscale* **2023**, *15*, 5305–5316. [CrossRef]
33. Jecny, J.; Huml, K. Structure of [1,3-bis(4-methoxyphenyl)-1,3-propanedionato](1,6-dichloro-1,5-cyclooctadiene)rhodium(I), $C_{25}H_{25}Cl_2O_4Rh$. *Acta Crystallogr. Sect. C* **1985**, *41*, 503–504. [CrossRef]
34. Macrae, C.F.; Sovago, I.; Cottrell, S.J.; Galek, P.T.A.; McCabe, P.; Pidcock, E.; Platings, M.; Shields, G.P.; Stevens, J.S.; Towler, M.; et al. Mercury 4.0: From visualization to analysis, design and prediction. *J. Appl. Crystallogr.* **2020**, *53*, 226–235. [CrossRef]
35. Pidluzhna, A.; Vembris, A.; Grzibovskis, R.; Zommere, M.A.; Bezvikonnyi, O.; Simokaitiene, J.; Baronaite, M.; Volyniuk, D.; Grazulevicius, J.V.; Ali, A.; et al. The Effect of Molecular Structure on the Properties of Fluorene Derivatives for OLED Applications. *Molecules* **2024**, *29*, 4918. [CrossRef]

36. Kuhn, A.; von Eschwege, K.G.; Conradie, J. Electrochemical and density functional theory modeled reduction of enolized 1,3-diketones. *Electrochim. Acta* **2011**, *56*, 6211–6218. [CrossRef]
37. Conradie, J.; Swarts, J.C. Relationship between electrochemical potentials and substitution reaction rates of ferrocene-containing β-diketonato rhodium(i) complexes; Cytotoxicity of [Rh(FcCOCHCOPh)(cod)]. *Dalton Trans.* **2011**, *40*, 5844–5851. [CrossRef] [PubMed]
38. Fourie, E.; Niemantsverdriet, J.W.; Swarts, J.C. Synthesis Comparative Electrochemistry and Spectroelectrochemistry of Metallocenyl β-Diketonato Dicarbonyl Complexes of Rhodium(I)—Cytotoxicity of [Rh(FcCOCHCOCF$_3$)(CO)$_2$]. *Inorganics* **2024**, *12*, 321. [CrossRef]
39. Nafady, A.; Chin, T.T.; Geiger, W.E. Manipulating the Electrolyte Medium to Favor Either One-Electron or Two-Electron Oxidation Pathways for (Fulvalendiyl)dirhodium Complexes. *Organometallics* **2006**, *25*, 1654–1663. [CrossRef]
40. Ramollo, G.K.; López-Gómez, M.J.; Liles, D.C.; Matsinha, L.C.; Smith, G.S.; Bezuidenhout, D.I. Rhodium(I) Ferrocenylcarbene Complexes: Synthesis, Structural Determination, Electrochemistry, and Application as Hydroformylation Catalyst Precursors. *Organometallics* **2015**, *34*, 5745–5753. [CrossRef]
41. Conradie, J.; Cameron, T.S.; Aquino, M.A.S.; Lamprecht, G.J.; Swarts, J.C. Synthetic, electrochemical and structural aspects of a series of ferrocene-containing dicarbonyl β-diketonato rhodium(I) complexes. *Inorganica Chim. Acta* **2005**, *358*, 2530–2542. [CrossRef]
42. *U. COSMO*, version 1.48; Bruker AXS Inc.: Madison, WI, USA, 2003.
43. Bruker. *SAINT-PLUS*, version 7.12; including XPREP; Bruker AXS Inc.: Madison, WI, USA, 2004.
44. *SADABS*, version 2016/2; Bruker AXS Inc.: Madison, WI, USA, 2016.
45. Sheldrick, G. SHELXT—Integrated space-group and crystal-structure determination. *Acta Crystallogr. Sect. A* **2015**, *71*, 3–8. [CrossRef] [PubMed]
46. Dolomanov, O.V.; Bourhis, L.J.; Gildea, R.J.; Howard, J.A.K.; Puschmann, H. OLEX2: A complete structure solution, refinement and analysis program. *J. Appl. Crystallogr.* **2009**, *42*, 339–341. [CrossRef]
47. Gritzner, G.; Kuta, J. Recommendations on reporting electrode potentials in nonaqueous solvents (Recommendations 1983). *Pure Appl. Chem.* **1984**, *56*, 461–466. [CrossRef]

Disclaimer/Publisher's Note: The statements, opinions and data contained in all publications are solely those of the individual author(s) and contributor(s) and not of MDPI and/or the editor(s). MDPI and/or the editor(s) disclaim responsibility for any injury to people or property resulting from any ideas, methods, instructions or products referred to in the content.